\



Uniform light emission from electrically driven plasmonic grating using multilayer tunneling barriers

Xiao-Bo He(何小波), Hua-Tian Hu(胡华天), Ji-Bo Tang(唐继博), Guo-Zhen Zhang(张国桢), Xue Chen(陈雪), Jun-Jun Shi(石俊俊), Zhen-Wei Ou(欧振伟), Zhi-Feng Shi(史志锋), Shun-Ping Zhang(张顺平), Chang Liu(刘昌), and Hong-Xing Xu(徐红星)

Citation: Chin. Phys. B, 2022, 31 (**1**): 017803. DOI: 10.1088/1674-1056/ac248f
Journal homepage: http://cpb.iphy.ac.cn; http://iopscience.iop.org/cpb

What follows is a list of articles you may be interested in

Efficiency droop in InGaN/GaN-based LEDs with a gradually varying In composition in each InGaN well layer

Shang-Da Qu(屈尚达), Ming-Sheng Xu(徐明升), Cheng-Xin Wang(王成新), Kai-Ju Shi(时凯居), Rui Li(李睿), Ye-Hui Wei(魏烨辉), Xian-Gang Xu(徐现刚), and Zi-Wu Ji(冀子武)

Chin. Phys. B, 2022, 31 (**1**): 017801. DOI: 10.1088/1674-1056/ac0817

Analysis of stress-induced inhomogeneous electroluminescence in GaN-based green LEDs grown on mesh-patterned Si (111) substrates with n-type AlGaN layer

Quan-Jiang Lv(吕全江), Yi-Hong Zhang(张一鸿), Chang-Da Zheng(郑畅达), Jiang-Dong Gao(高江东), Jian-Li Zhang(张建立), Jun-Lin Liu(刘军林)

Chin. Phys. B, 2020, 29 (**8**): 087801. DOI: 10.1088/1674-1056/ab96a2

Optoelectronic properties analysis of silicon light-emitting diode monolithically integrated in standard CMOS IC

Yanxu Chen(陈彦旭), Dongliang Xu(许栋梁), Kaikai Xu(徐开凯), Ning Zhang(张宁), Siyang Liu(刘斯扬), Jianming Zhao(赵建明), Qian Luo(罗谦), Lukas W. Snyman, Jacobus W. Swart

Chin. Phys. B, 2019, 28 (**10**): 107801. DOI: 10.1088/1674-1056/ab3e44

Characteristic improvements of thin film AlGaInP red light emitting diodes on a metallic substrate

Bin Zhao(赵斌), Wei Hu(胡巍), Xian-Sheng Tang(唐先胜), Wen-Xue Huo(霍雯雪), Li-Li Han(韩丽丽), Ming-Long Zhao(赵明龙), Zi-Guang Ma(马紫光), Wen-Xin Wang(王文新), Hai-Qiang Jia(贾海强), Hong Chen(陈弘)

Chin. Phys. B, 2018, 27 (**4**): 047803. DOI: 10.1088/1674-1056/27/4/047803

High mobility ultrathin ZnO p-n homojunction modulated by $Zn_{0.85}Mg_{0.15}O$ quantum barriers

Jing-Jing Yang(杨景景), Qing-Qing Fang(方庆清), Wen-Han Du(杜文汉), Ke-Ke Zhang, Da-Shun Dong(董大舜)

Chin. Phys. B, 2018, 27 (**3**): 037804. DOI: 10.1088/1674-1056/27/3/037804

Uniform light emission from electrically driven plasmonic grating using multilayer tunneling barriers

Xiao-Bo He(何小波)[1,2], Hua-Tian Hu(胡华天)[3], Ji-Bo Tang(唐继博)[3], Guo-Zhen Zhang(张国桢)[1], Xue Chen(陈雪)[1], Jun-Jun Shi(石俊俊)[2], Zhen-Wei Ou(欧振伟)[1], Zhi-Feng Shi(史志锋)[4], Shun-Ping Zhang(张顺平)[1,†], Chang Liu(刘昌)[1,‡], and Hong-Xing Xu(徐红星)[1,3,§]

[1] *School of Physics and Technology, Center for Nanoscience and Nanotechnology, and Key Laboratory of Artificial Micro- and Nano-structures of Ministry of Education, Wuhan University, Wuhan* 430072, *China*

[2] *Shandong Provincial Engineering and Technical Center of Light Manipulation and Shandong Provincial Key Laboratory of Optics and Photonic Devices, School of Physics and Electronics, Shandong Normal University, Jinan* 250014, *China*

[3] *The Institute for Advanced Studies, Wuhan University, Wuhan* 430072, *China*

[4] *Key Laboratory of Materials Physics of Ministry of Education, School of Physics and Microelectronics, Zhengzhou University, Zhengzhou* 450052, *China*

(Received 24 March 2021; revised manuscript received 16 June 2021; accepted manuscript online 8 September 2021)

Light emission by inelastic tunneling (LEIT) from a metal–insulator–metal tunnel junction is an ultrafast emission process. It is a promising platform for ultrafast transduction from electrical signal to optical signal on integrated circuits. However, existing procedures of fabricating LEIT devices usually involve both top-down and bottom-up techniques, which reduces its compatibility with the modern microfabrication streamline and limits its potential applications in industrial scale-up. Here in this work, we lift these restrictions by using a multilayer insulator grown by atomic layer deposition as the tunnel barrier. For the first time, we fabricate an LEIT device fully by microfabrication techniques and show a stable performance under ambient conditions. Uniform electroluminescence is observed over the entire active region, with the emission spectrum shaped by metallic grating plasmons. The introduction of a multilayer insulator into the LEIT can provide an additional degree of freedom for engineering the energy band landscape of the tunnel barrier. The presented scheme of preparing a stable ultrathin tunnel barrier may also find some applications in a wide range of integrated optoelectronic devices.

Keywords: electroluminescence, plasmonics, inelastic electron tunneling, multilayer insulator, atomic layer deposition

PACS: 78.60.Fi, 78.66.–w

DOI: 10.1088/1674-1056/ac248f

1. Introduction

Light emission by inelastic tunneling (LEIT) through a tunnel junction can offer unique opportunities to realize ultrafast electrical-optical-signal transduction,[1,2] which can generate light below the diffraction limit and provide potential applications in nanoscale biosensing,[3,4] optical communication,[5] and integrated photonics circuits.[6] First demonstrated by Lambe and McCarthy in 1976,[7] the tunneling electrons in a planar metal–insulator–metal (MIM) tunnel junction will excite the surface plasmons and may subsequently decay into far-field photons. This luminescence process is in principle ultrafast because the timescale for an electron tunneling through the junction proves to be on the order of 10 fs (the excitation process), and the lifetime of an emitter in the nanogap can be shortened to tens of fs (the emission process).[8,9] This phenomenon is then used to visualize the local density of states in scanning tunneling microscopes[10–13] until recently it has received considerable renewed interest in electrically-driven optical antennas.[14,15] Significant advances have been made since then, including the improvement of the emission efficiency,[16,17] radiation directionality,[18] and spectra shape[19–21] of the MIM tunnel sources. The stability of an LEIT device, a key operation figure of merit, depends significantly on the fabrication of the tunnel barrier. Till now, a highly stable tunnel barrier has relied mainly on the synthesis of a dense insulator layer between the biased metal structures, by, *e.g.*, thermal oxide,[22] exfoliated hexagonal boron nitride,[23] or self-assemble molecules.[24] However, these methods are either hard to control the thickness (oxidization) or incompatible with the modern microfabrication streamline, hindering the LEIT devices from being manufactured and put into practical applications.

Atomic layer deposition (ALD) is a well-developed technique of depositing thin films in microelectronics,[25,26] light-emitting diodes,[27] hot-electron electrochemistry,[28] and diffusion barrier coatings with low gas permeability.[29] The uniqueness of ALD in these applications is attributed to its ability to grow the uniform, pinhole-free, and nanometer-thick

†Corresponding author. E-mail: spzhang@whu.edu.cn
‡Corresponding author. E-mail: chang.liu@whu.edu.cn
§Corresponding author. E-mail: hxxu@whu.edu.cn

© 2022 Chinese Physical Society and IOP Publishing Ltd

insulator layers.[30,31] However, the operation of LEIT devices with a single Al_2O_3 layer grown by ALD is unstable under ambient condition due to the formation of grains and defects during the growing process.[32] Therefore, it is necessary to obtain high-quality tunnel insulators by ALD so that the fabrication of LEIT devices is fully compatible with microfabrication techniques.

2. Method

2.1. Device fabrication

Electrically driven plasmonic gratings are fabricated on Si/SiO_2 substrate. The thickness of the SiO_2 layer is 300 nm that can efficiently reduce the leak current. The bottom Au electrode is prepared by a series of fabrication steps, including EBL, reaction-ion etching (RIE, using CHF_3 gas flow), and thermal evaporation of Au film (50 nm). After lift-off, the O_2 plasma treatment process in an RIE is used to generate the high hydroxyl density substrate, in which the treatment power is 50 W and the treatment time is 1 min. The treated sample is then grown on the multiple insulator layers by ALD at a temperature of 150 °C. Then, the top gratings are prepared by the EBL, Au evaporation, and lift-off. The details of the fabrication process are shown in the supporting information, Fig. S1.

2.2. Electrical and optical characterization

For electrical measurements, two tungsten probes with 10-μm diameter are used to contact the Au electrodes with a sourcemeter (Keithley 2634B). The parameters are 5 NPLC (number of power line cycles) for the analog-to-digital converter, integration times of 1 s, and the current using the automatic range switch. The EL images are recorded by an optical microscope (Olympus BX51) equipped with a 50× long working distance objective (NA = 0.5) and a CCD camera (DVC 710M-00-MW). The emission spectrum is collected by a spectrometer (Andor 550i, 150 lines/mm blazing at 800 nm) and detected by the EMCCD (Andor Newton). The reflection spectrum is collected by a home-built microscope using a 100× objective (NA = 0.9) and the diameter of the white light spot is 2 μm.

2.3. Electromagnetic simulations

Full wave electromagnetic simulations are carried out by commercial FEM software (COMSOL Multiphysics, V5.2a). A two-dimensional model is established by considering the grating positioned on the top of an Au film. The permittivity of Au is cited from the Johnson and Christy.[40] The insulator gaps within the structures have a thickness of 4.0 nm and a refractive index of 2.05.

3. Experiment and results

In this work, we fabricate an LEIT device with uniform light emission and a long working lifetime under ambient condition, by optimizing the composition during the ALD growth. For the first time, we grow alternative insulator layers (TiO_2–Al_2O_3–TiO_2–Al_2O_3) as the tunnel barrier, in a fully microfabrication-compatible manner. Our devices can be stored for a long time (several weeks) and the tunneling current keeps stable for intermittent measurements from hours to days. The light emission is uniform in the entire active region, and the emission spectra can be controlled by a plasmonic grating. Our study demonstrates that the multilayer insulators grown by ALD enable a stable and uniform LEIT device. Furthermore, the composite tunnel barrier may also provide an additional degree of freedom for the band structure of the tunnel barrier[33,34] or find applications in other ultrafast electro-optical circuits. Figure 1(a) shows the schematic of an LEIT device. It consists of a square bottom Au electrode, alternate insulator (TiO_2–Al_2O_3) layers, and a top Au plasmonic grating simultaneously serving as a coupler for light and a positive electrode. The bottom Au electrode and the top plasmonic grating are prepared by electron beam lithography (EBL), and both layers are 50-nm thick. The grating is aligned accurately to the bottom square electrode during the exposure. Thealternate insulator layers are deposited by ALD, including 18 cycles (0.8 nm) of TiO_2, 8 cycles (0.8 nm) of Al_2O_3, 18 cycles (0.8 nm) of TiO_2, and 16 cycles (1.6 nm) of Al_2O_3. The total thickness of the four layers is 4 nm. The entire fabrication process fits well with the modern microfabrication streamline (for details see supporting information Fig. S1). The inset of Fig. 1(a) shows a side view of the active region, where the silicon substrate is not shown.

The energy band diagram of the MIM junction with and without bias voltage is shown in Fig. 1(b). There are five potential barrier interfaces between Au electrodes. The shape of the energy band diagram of tunnel barriers is determined by the work function of the Au electrode (5.1 eV),[35] the electron affinity of insulator, and the applied bias voltage. The electron affinity potential of TiO_2 and Al_2O_3 depend on the thickness and morphology of the film,[36] and are estimated to be 4.3 eV and 3.5 eV from the ALD process. The barrier height of interface at the zero bias is determined to be $\Phi_1 = 0.8$ eV for Au–TiO_2 interface, $\Phi_2 = 1.6$ eV for Au–Al_2O_3 interface, and $\Phi_3 = 0.8$ eV for TiO_2–Al_2O_3 interfaces,as shown in the upper panel of Fig. 1(b). When electrons tunnel over the insulator barrier under the bias voltage, part of electrons will undergo the inelastic scattering and lose their energy by generating a plasmon, subsequently radiating photons or creating heat in the local region. By changing the height, period, duty cycle of the grating and the thickness of the alternate insulators, the spectrum and polarization of the electroluminescence can be

controlled. Comparing with the tunneling junctions with single insulators, the choice of two or more insulators facilitates the design of both the electronic and photonic aspects of the devices. For example, the tunneling current can be larger for such an alternate insulator junction than the counterpart of a pure Al_2O_3 junction with equal thickness. For a given tunneling current, a multilayer junction can sustain a higher damage voltage, which is a key to a stable light emission by inelastic tunneling device. Unlike traditional light sources, the emission process of LEIT does not rely on the spontaneous recombination of electron–hole pairs. The response time of the emission can decrease down to tens of femtosecond, dependent mainly on the electron tunneling process and the subsequent radiative decay of the plasmons.[37] These enable the light emission by inelastic tunneling to become a component of an integrated ultrafast optoelectronic circuit.

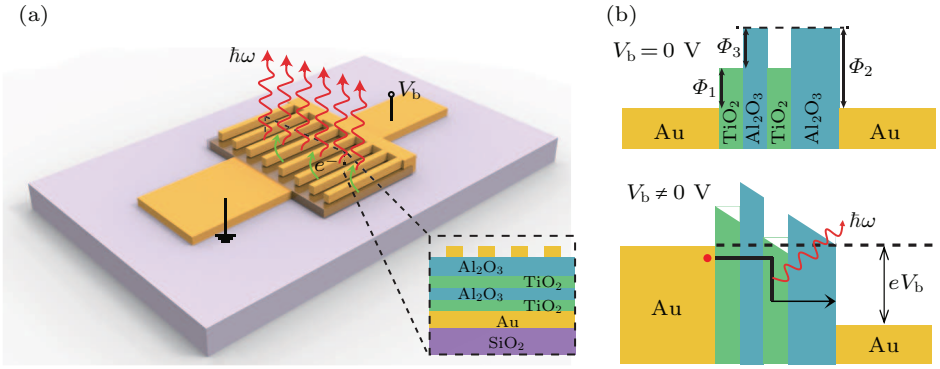


Fig. 1. (a) Schematic diagram of the device. The inset shows a side view of active region (unscaled), and contains, from bottom to top, a silica substrate, a square Au bottom electrode, alternative insulator layers, and an Au grating. The 50-nm-thick gratings are fabricated onto the bottom electrode with a 4-nm-thick tunnel barrier of TiO_2&Al_2O_3 grown in between. (b) Energy band diagram of multilayer tunnel junction with zero and positive bias, with Φ_i ($i = 1, 2, 3$) denoting barrier height, V_b applied voltage, and $\hbar\omega$ light emission.

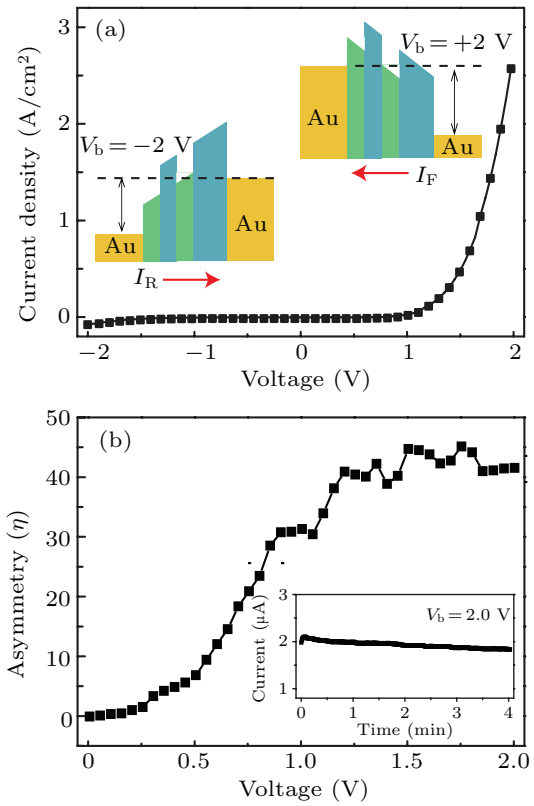


Fig. 2. (a) Current–voltage characteristic curve of connected plasmonic grating device with a tunneling gap, where insets show energy band diagrams of multilayer tunneling junction with a negative or positive bias applied to top Au electrode. (b) Asymmetry ($\eta = |I_F/I_R|$) *versus* bias voltage for the MIM tunnel diode, where inset displays time trace of tunneling current at a constant bias of $V_b = 2.0$ V with tunnel junction size being 60 μm^2.

The tunneling current of our device is determined by both the amplitude and the direction of the applied voltage since there are multiple insulators with different electron affinities in the tunnel barrier. The characteristic of current density (J) as a function of the applied voltage is shown in Fig. 2(a). A pronounced asymmetry appears when the direction of injection electrons is reversed. The inset of Fig. 2(a) presents the energy band diagram with negative and positive voltage. When applying a positive bias voltage of +2 V to the top Au electrode, the width of the TiO_2&Al_2O_3 tunnel barrier is smaller than that when applying a negative bias of −2 V. Hence, the positive current density is greater than the negative one at the MIM tunnel junction. In the following, we always use a positive bias in the LEIT measurements since the intensity of emission photons depends linearly on the amplitude of the tunnel current.[20] Supporting information figure S2 also shows that the tunneling current increases linearly with the augment of area of the junction.

We now come to study the asymmetry of the current *versus* voltage (I–V) curve and the stability of the tunnel junctions. The asymmetry of the I–V curve is defined as the forward current divided by the reverse current ($\eta = |I_F/I_R|$), which presents the characterization of rectification for a tunnel MIM diode. Figure 2(b) shows that the value of asymmetry is related to the value of applied voltage. The asymmetry value of the tunnel junction reaches 45 when $|V_b| = 2$ V. The inset of Fig. 2(b) shows the time trace of the tunneling current of the MIM junction with a junction size of 60 μm^2 at a bias voltage of 2.0 V. The tunneling current keeps stable during the measurement, guaranteeing key feature required in further applications (*e.g.*, optoelectronic circuits). Stabler devices can be

achieved by packaging the final device or utilizing the transferred top Au nanostructure (electrodes).[38]

The optical characterization of the tunneling device and the emission spectra of the LEIT source are determined by the resonance properties of the grating. The reflection spectra are measured in the home-built microscope (for details, see supporting information Fig. S3). Considering that the plasmon resonance has a smaller loss in the near-infrared region,[37] the grating is designed with a duty cycle of 0.5 and a period of 700 nm. Figure 3(a) shows the reflection spectra from the grating under perpendicular and parallel polarization. The grating shows a strong polarization response, an apparent reflection dip at 770 nm shows up under perpendicular polarization. The polarization dependence of EL spectrum presents a similar behavior, with the emitted photon polarized perpendicular to the grating (supporting information, Fig. S6).The inset of Fig. 3(a) shows the scanning electron microscopy images of the same devices. Numerical simulations of the grating nanostructure are in good agreement with the experimental result as shown in Fig. 3(b). The inset shows a side view of the electric field distribution of a grating at the resonant wavelength. High enhancement of the electric field is confined in the tunnel junction and at the top edge of the grating, which conduces to improving the efficiency of LEIT device.

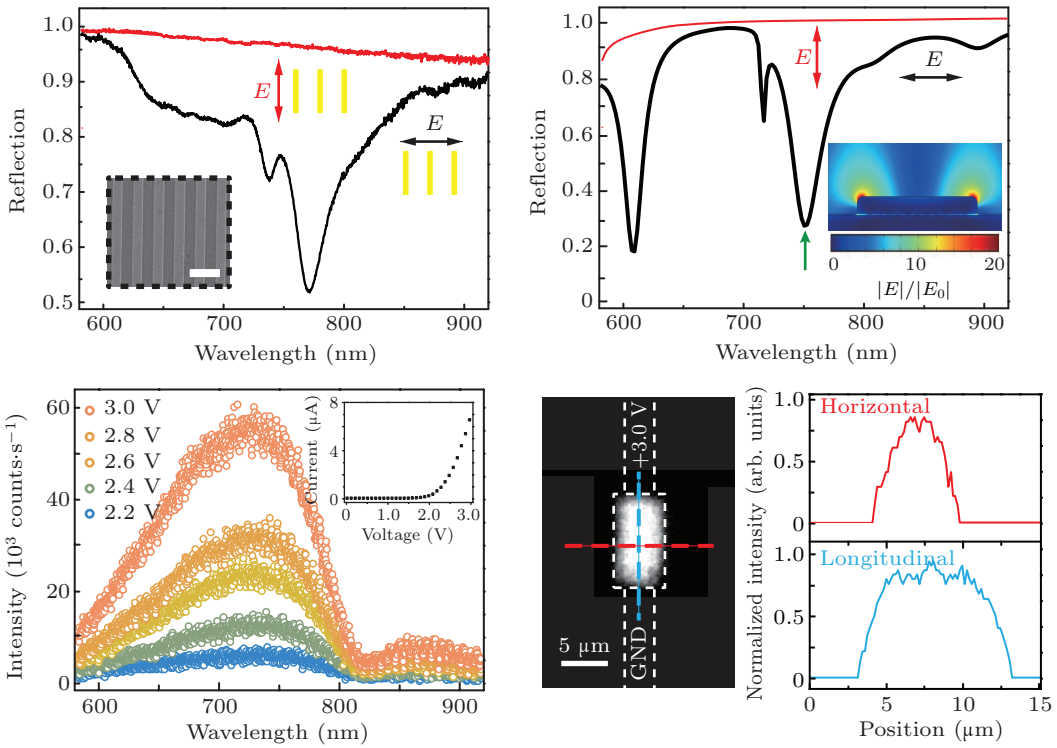


Fig. 3. (a) Reflection spectra of grating under parallel (red) and perpendicular (black) excitation. Inset shows scanning electron microscope image of the grating. It has a duty cycle of 0.5 and a period of 700 nm. Scale bar: 1 μm. (b) Simulated reflection spectra of the grating under parallel (red) and perpendicular excitation. The inset shows the electric field distribution under the resonance condition with a wavelength of 750 nm. (c) EL spectra of the grating for various applied voltages. The inset shows the *I*–*V* curve of the device. (d) Image of light emitted from the grating at a constant bias of $V_b = 3.0$ V. The CCD exposure time is 3 s. The right panels indicate the intensity profiles along the major axis and minor axis of the EL image, corresponding to the dashed line on the left panel.

Next, we explore the properties of the emission light from the electrically driven grating. We use two tungsten probes connected with a sourcemeter to apply the bias voltage to the device. Light emission from the tunneling junction is collected by a long working distance objective (Olympus, 50×, NA = 0.5) and then recorded by a CCD camera or by a spectrometer (for details, see Methods). All measurements are conducted at room temperature. Figure 3(c) shows the emission spectra with various bias voltages, the intensity of EL peak becomes stronger with voltage increasing. The peak position of EL spectrum is 728 nm, which fits well with the reflection spectrum. We note that the drop of the EL spectrum at about 820 nm is not caused by the experimental collection system. It may be due to the lower electric field enhancement in the tunnel junction and at the top edge of the grating, corresponding to a weak radiation efficiency at the dip (∼ 840 nm) in the reflection spectrum in Fig. 3(b) (also see supporting information Fig. S7). The inset of Fig. 3(c) shows the corresponding *I*–*V* curves of the same device. Figure 3(d) shows the direct imaging of light emitted from gratings at a constant bias voltage of $V_b = 3.0$ V. The intensity of the emission spot is uniform, which shows that the tunneling electrons uniformly pass through the barrier of the MIM junction. The right panels show that the intensity profiles along the different axes of the tunnel source, and there appear only small fluctuations from different positions. Supporting information Fig. S5 shows the

photon emission from a planar MIM tunnel junction, and the emitted photons are observed only from the edges of the top electrode. The external conversion efficiency of the electron-to-photon of the light source is estimated at about 3.8×10^{-6} at $V_b = 3.0$ V, following the same procedure as in our previous work.[20]

4. Conclusions

In this work, we demonstrate electrically driven plasmonic gratings based on a multilayer tunneling barrier grown by ALD, where the source shows stable and uniform emission characteristics. Four insulator layers are utilized to fabricate the MIM tunneling sources for the first time. It shows that the tunneling probability of one electron is dependent on the injection direction due to the utilization of the multiple insulators with different electron affinities in one tunnel barrier. The tunneling probability of the electrons from the bottom Au electrode is much higher than that from the top grating. The problem of poor stability of the ultrathin insulator layer grown by ALD in the MIM tunnel source is solved by utilizing multilayer barriers. According to Ref. [39], the resonant electron tunneling based on multilayer barriers may happen and will further enhance the efficiency.[39] Our work paves the way for fabricating a stabler and efficient subwavelength LEIT device, which is of potential significance in implmenting the on-chip optical communication, biosensing, and photodetection.

Acknowledgements

Project supported by the National Natural Science Foundation of China (Grant Nos. 12004222 and 91850207), the National Key Research and Development Program of China (Grant Nos. 2017YFA0303504 and 2017YFA0205800), the Fundamental Research Funds for the Central Universities, China, the Strategic Priority Research Program of Chinese Academy of Sciences (Grant No. XDB30000000), and the Postdoctoral Science Foundation of China (Grant No. 2020M682223).

References

[1] Parzefall M and Novotny L 2019 *Rep. Prog. Phys.* **82** 112401
[2] Liu L F, Xu Y, Zhu J J, Wang P, Tong L M and Krasavin A V 2020 *Frontiers in Physics* **8** 251
[3] Dathe A, Ziegler M, Hübner U, Fritzsche W and Stranik O 2016 *Nano Lett.* **16** 5728
[4] Wang P, Nasir M E, Krasavin A V, Dickson W and Zayats A V 2020 *Nano Lett.* **20** 1536
[5] Kullock R, Ochs M, Grimm P, Emmerling M and Hecht B 2020 *Nat. Commun.* **11** 115
[6] Du W, Wang T, Chu H-S and Nijhuis C A 2017 *Nat. Photon.* **11** 623
[7] Lambe J and McCarthy S L 1976 *Phys. Rev. Lett.* **37** 923
[8] Shafir D, Soifer H, Bruner B D, Dagan M, Mairesse Y, Patchkovskii S, Ivanov M Y, Smirnova O and Dudovich N 2012 *Nature* **485** 343
[9] Zhang Y, Chen W, Fu T, Sun J, Zhang D, Li Y, Zhang S and Xu H 2019 *Nano Lett.* **19** 6284
[10] Chen C, Bobisch C and Ho W 2009 *Science* **325** 981
[11] Dong Z C, Zhang X L, Gao H Y, Luo Y, Zhang C, Chen L G, Zhang R, Tao X, Zhang Y, Yang J L and Hou J G 2009 *Nat. Photon.* **4** 50
[12] Bharadwaj P, Bouhelier A and Novotny L 2011 *Phys. Rev. Lett.* **106** 226802
[13] Krane N, Lotze C, Läger J M, Reecht G and Franke K J 2016 *Nano Lett.* **16** 5163
[14] Parzefall M, Bharadwaj P, Jain A, Taniguchi T, Watanabe K and Novotny L 2015 *Nat. Nanotechnol.* **10** 1058
[15] Kern J, Kullock R, Prangsma J, Emmerling M, Kamp M and Hecht B 2015 *Nat. Photon.* **9** 582
[16] Namgung S, Mohr D A, Yoo D, Bharadwaj P, Koester S J and Oh S H 2018 *ACS Nano* **12** 2780
[17] Qian H L, Hsu S W, Gurunatha K, Riley C T, Zhao J, Lu D, Tao A R and Liu Z W 2018 *Nat. Photon.* **12** 485
[18] Gurunarayanan S P, Verellen N, Zharinov V S, James Shirley F, Moshchalkov V V, Heyns M, Van de Vondel J, Radu I P and Van Dorpe P 2017 *Nano Lett.* **17** 7433
[19] Vardi Y, Cohen-Hoshen E, Shalem G and Bar-Joseph I 2016 *Nano Lett.* **16** 748
[20] He X, Tang J, Hu H, Shi J, Guan Z, Zhang S and Xu H 2019 *ACS Photon.* **6** 823
[21] Qin J, Liu Y, Luo H, Jiang Z, Cai W and Wang L 2019 *ACS Photon.* **6** 2392
[22] Zhang C, Hugonin J P, Coutrot A L, Sauvan C, Marquier F and Greffet J J 2019 *Nat. Commun.* **10** 4949
[23] Parzefall M, Szabo A, Taniguchi T, Watanabe K, Luisier M and Novotny L 2019 *Nat. Commun.* **10** 292
[24] He X, Tang J, Hu H, Shi J, Guan Z, Zhang S and Xu H 2019 *ACS Nano* **13** 14041
[25] Zhang G, Guo T, He X, Ai Z, Wu H and Liu C 2018 *Adv. Electron. Mater.* **4** 1800195
[26] Cho T H, Farjam N, Allemang C R, Pannier C P, Kazyak E, Huber C, Rose M, Trejo O, Peterson R L, Barton K and Dasgupta N P 2020 *ACS Nano* **14** 17262
[27] Li D, Cheng R, Zhou H, Wang C, Yin A, Chen Y, Weiss N O, Huang Y and Duan X 2015 *Nat. Commun.* **6** 7509
[28] Chae H U, Ahsan R, Lin Q, Sarkar D, Rezaeifar F, Cronin S B and Kapadia R 2019 *Nano Lett.* **19** 6227
[29] George S M 2010 *Chem. Rev.* **110** 111
[30] Cowell E W, 3rd, Alimardani N, Knutson C C, Conley J F Jr, Keszler D A, Gibbons B J and Wager J F 2011 *Adv. Mater.* **23** 74
[31] Periasamy P, Guthrey H L, Abdulagatov A I, Ndione P F, Berry J J, Ginley D S, George S M, Parilla P A and O'Hayre R P 2013 *Adv. Mater.* **25** 1301
[32] Kirtley J, Theis T N and Tsang J C 1981 *Phys. Rev. B* **24** 5650
[33] Sze S M and Ng K K 2006 *Physics of semiconductor devices* (John Wiley & Sons)
[34] Grover S and Moddel G 2012 *Solid-State Electronics* **67** 94
[35] Aydinoglu F, Alhazmi M, Cui B, Ramahi O, Irannejad M and Yavuz M 2013 *Austin J. Nanomed. Nanotechnol* **1** 1
[36] Tien T C, Pan F M, Wang L P, Lee C H, Tung Y L, Tsai S Y, Lin C, Tsai F Y and Chen S J 2009 *Nanotechnology* **20** 305201
[37] Parzefall M and Novotny L 2018 *ACS Photon.* **5** 4195
[38] Liu Y, Guo J, Zhu E, Liao L, Lee S J, Ding M, Shakir I, Gambin V, Huang Y and Duan X 2018 *Nature* **557** 696
[39] Uskov A V, Khurgin J B, Protsenko I E, Smetanin I V and Bouhelier A 2016 *Nanoscale* **8** 14573
[40] Johnson P B and Christy R W 1972 *Phys. Rev. B* **6** 4370